



ALMA MATER STUDIORUM  
UNIVERSITÀ DI BOLOGNA

ARCHIVIO ISTITUZIONALE  
DELLA RICERCA

## Alma Mater Studiorum Università di Bologna Archivio istituzionale della ricerca

Effects of rising damp and salt crystallization cycles in FRCM-masonry interfacial debonding: Towards an accelerated laboratory test method

This is the final peer-reviewed author's accepted manuscript (postprint) of the following publication:

*Published Version:*

Effects of rising damp and salt crystallization cycles in FRCM-masonry interfacial debonding: Towards an accelerated laboratory test method / Franzoni, Elisa; Gentilini, Cristina\*; Santandrea, Mattia; Carloni, Christian. - In: CONSTRUCTION AND BUILDING MATERIALS. - ISSN 0950-0618. - STAMPA. - 175:(2018), pp. 225-238. [10.1016/j.conbuildmat.2018.04.164]

*Availability:*

This version is available at: <https://hdl.handle.net/11585/636182> since: 2019-02-25

*Published:*

DOI: <http://doi.org/10.1016/j.conbuildmat.2018.04.164>

*Terms of use:*

Some rights reserved. The terms and conditions for the reuse of this version of the manuscript are specified in the publishing policy. For all terms of use and more information see the publisher's website.

This item was downloaded from IRIS Università di Bologna (<https://cris.unibo.it/>).  
When citing, please refer to the published version.

(Article begins on next page)

This is the final peer-reviewed accepted manuscript of:

Elisa Franzoni, Cristina Gentilini, Mattia Santandrea, Christian Carloni, *Effects of rising damp and salt crystallization cycles in FRCM-masonry interfacial debonding: Towards an accelerated laboratory test method*, Construction and Building Materials, Volume 175, 2018, Pages 225-238

ISSN 0950-0618

The final published version is available online at:

<https://doi.org/10.1016/j.conbuildmat.2018.04.164>

© 2018. This manuscript version is made available under the Creative Commons Attribution-NonCommercial-NoDerivs (CC BY-NC-ND) 4.0 International License (<http://creativecommons.org/licenses/by-nc-nd/4.0/>)

# Effects of rising damp and salt crystallization cycles in FRCM-masonry interfacial debonding: towards an accelerated laboratory test method

Elisa Franzoni<sup>1a</sup>, Cristina Gentilini<sup>2b\*</sup>, Mattia Santandrea<sup>3c</sup>, Christian Carloni<sup>4c</sup>

<sup>a</sup>DICAM – Department of Civil, Chemical, Environmental and Materials Engineering, University of Bologna,  
Via Terracini 28, 40129 Bologna, Italy

<sup>b</sup>DA – Department of Architecture, University of Bologna, Viale del Risorgimento 2, 40136 Bologna, Italy

<sup>c</sup>DICAM – Department of Civil, Chemical, Environmental and Materials Engineering, University of Bologna,  
Viale del Risorgimento 2, 40136 Bologna, Italy

<sup>1</sup>elisa.franzoni@unibo.it, <sup>2\*</sup>corresponding author: cristina.gentilini@unibo.it, <sup>3</sup>mattia.santandrea3@unibo.it,

<sup>4</sup>christian.carloni@unibo.it

**Keywords:** Bond strength; Natural hydraulic lime-based matrix; Direct-shear test; FRCM composite; Moisture; Porosity; Salt resistance; Durability; Masonry.

## Abstract

Fiber-reinforced composites with inorganic matrix (FRCMs) have been recently proposed as a more compatible and durable route to strengthen masonry structures with respect to FRPs (fiber-reinforced polymers), but their weathering mechanisms in aggressive environments are still scarcely known.

In this paper, brick masonry specimens were reinforced with FRCM strips, made of galvanized steel fibers embedded within a hydraulic lime-based mortar, and were subjected to an artificial weathering procedure designed by the authors, involving capillary water absorption and salt crystallization cycles. Finally, direct shear tests were performed on the FRCM-masonry joints.

To reproduce conditions that may be found in real buildings, shear tests were also carried out after applying the FRCM composite on salt laden masonry blocks.

Interfacial debonding behavior was interpreted based on the salt distribution within the masonry joints and the porosity of materials. The permeable matrix did not hinder the migration of the saline solution used in

some cycles, which in turn resulted in no significant accumulation of salts beneath the composite strip, and no micro-crack opening in the composite after accelerated weathering. Some corrosion of the galvanized steel cords in presence of high amount of chlorides was observed in the composite.

## **1. Introduction**

Masonry structures constitute a large part of the existing building stock in Europe and worldwide, and in particular of heritage buildings, which need to be preserved from natural disasters, deterioration, and anthropogenic damages. Historical masonry buildings, due to their construction technology, transformations undergone during time, materials weathering and other factors, are known to be particularly vulnerable to seismic events, as the recent Italian earthquakes demonstrated [1-5]. To prevent an extensive damage or even a complete disruption of ancient masonry buildings due to earthquakes, strengthening interventions with fiber reinforced polymer (FRP) composites were introduced more than two decades ago [6]. Strips of composites can be externally bonded to walls, columns, and arches in an attempt to modify the failure mechanisms of unreinforced masonry structures during earthquakes and thus increase the seismic resistance. Several studies have shown the effectiveness of FRP composites to strengthen masonry buildings provided that a good adhesion to the substrate is ensured, which is often a challenging task in real structures that are deteriorated [7-9]. The possibility to design their shape and fiber arrangement is one of the advantages of this technology, which allows to come up with a tailored solution for an existing building that requires a structural upgrade. To some extent, FRP composites are satisfactory also in terms of compatibility with the existing masonry, as their limited weight (when compared, for example, with steel-based strengthening solutions) does not significantly alter the overall weight of the building. In addition, given their limited thickness, FRP composites can be applied for example to arch extrados or under the plaster, which is an advantage in heritage buildings. Nevertheless, FRPs also exhibit an important drawback connected to durability, as the organic resins used in the matrix are subject to ageing due to moisture, UV radiation, oxygen, temperature, and other environmental factors [10-12]. To overcome this limitation, strengthening systems based on inorganic matrices, the so-called fiber reinforced cementitious matrix (FRCM) composites, have been introduced [13-15]. An FRCM system

consists of a sheet of fibers embedded in a grout that can be cementitious-based or lime-based. The fibers are usually made of carbon, steel, basalt, glass, or polyparaphenylene benzobisoxazole. The use of an inorganic matrix allows to overcome some of the drawbacks of the FRPs, as the grout can be more easily applied to irregular substrates, is less susceptible to ageing and is permeable to water and water vapor, the latter being a key issue in historical masonry, which is often characterized by some moisture from soil (rising damp), condensation (due to limited thermal insulation of old walls), wind-driven rain, or infiltrations [16, 17]. Preventing such moisture from evaporating may result in severe deterioration patterns or even in the detachment of scarcely permeable layers from the surface, which could be a hurdle to the adhesion of the composite strips that are applied to the surface itself. Also in terms of durability, FRCM composites are expected to provide a better long-term behavior when compared to FRPs. However, the response of FRCM composites to weathering is still mostly unexplored and there is a strong need for a better understanding of the possible deterioration mechanisms affecting FRCM composites and, even more important, the FRCM-masonry 'system'.

So far, very few studies investigated these aspects and no guidelines, standards, or codes of practice exist yet on this subject. Although some recommendations were issued in the past on the durability assessment of FRPs, they cannot be extended to FRCM composites, as the latter ones are supposed to be vulnerable to entirely different deterioration processes when compared to FRPs. In particular, FRCMs are expected not to suffer from hot climates and solar radiation, but their porosity makes them possibly vulnerable, for example, to moisture-related damage, as salt crystallization cycles and other processes [18-21]. The presence of salts is very common in historical buildings and it is a major cause of damage, as highlighted in the literature (see [22, 23]).

In a previous paper by the authors [24], a preliminary experimental campaign was carried out to investigate the bond behavior of steel FRCM strips applied to fired-clay brick masonry blocks subjected to salt crystallization cycles. The study was aimed at contributing to the assessment of the durability of FRCM systems applied to masonry in presence of salt attack. The present paper represents a step forward with respect to the previous research effort [24], as it will be explained in Section 2.

## 2. Background and research aims

In a recent paper [24], an experimental procedure to investigate the salt resistance of steel FRCM composites applied to masonry blocks was developed and evaluated by the authors. Briefly, the procedure consisted of the following steps:

- Steel FRCM strips embedded in a natural hydraulic lime-based grout were applied to masonry blocks (made of 6 half-bricks and 5 mortar joints) and left to cure;
- The steel FRCM-masonry joints were partially or totally wrapped by means of duct tape. In the partially wrapped specimens, evaporation (and hence salt crystallization) was forced to occur through the entire top face of the masonry block where the composite strip was applied: while in the totally wrapped specimens, evaporation occurred only through the FRCM strip;
- Four accelerated weathering cycles were performed. Each cycle comprised a phase of capillary absorption of a sodium sulfate decahydrate solution (specimens were positioned with the FRCM strip upwards) and a phase of drying (in ventilated oven);
- The same four cycles were performed in deionized water, to assess the role of wetting-drying cycles alone on the curing process of the FRCM matrix and hence to separate the effect of salt from the effect of water alone;
- Single-lap shear tests were carried out to assess the bond capacity between FRCM and masonry in not-weathered (control) and weathered conditions;
- The salt distribution and the porosity at different locations throughout the specimens were determined, to investigate the transport mechanisms of the saline solution and its possible deteriorating action.

The research highlighted that the matrix employed for the FRCM system, based on natural hydraulic lime, allowed the transport of the saline solution through the composite, leading to the accumulation of efflorescence on the external surface of the composite rather than the precipitation of sub-efflorescence. As a consequence, no damage or decrease of bond capacity was observed in the conditioned FRCM-masonry joints. The water used in the cycles had a slightly beneficial effect on the curing process of the hydraulic lime-

based matrix, which confirmed the importance of analyzing separately the effect of salt and water. No significant differences were found in the salt distribution between the partially wrapped and totally wrapped specimens.

Based on these preliminary results, in this paper a new experimental campaign is undertaken, which employs the same experimental set-up, to introduce some key advances:

- A mix of sodium sulfate and sodium chloride, more representative of the salts found in real historical masonry, is used for the saline solution;
- Six weathering cycles are carried out instead of four, in order to make the accelerated weathering more aggressive;
- Two entirely new conditions are considered in this study, in order to investigate the case of FRCM composite strips applied to an existing masonry structure that is *already* affected by the presence of moisture and salts, which is a typical scenario in practical applications:
  - a) steel FRCM strips are applied to salt-laden masonry blocks, i.e. blocks that have been previously subjected to wetting-drying cycles in the same saline solution;
  - b) direct shear test is performed on water-saturated FRCM-masonry joints (that have been subjected to wetting-drying cycles in deionized water), to assess the influence of water in the material pores on the mechanical behavior of the composite.

The study is aimed not only at assessing the bond capacity of the FRCM-masonry joints subjected to accelerated weathering, but also to investigate the mechanisms of salts migration and accumulation across the specimens and to contribute to the development of a standardized laboratory method for this purpose.

### **3. Materials and methods**

#### **3.1. Materials and specimens**

Nineteen masonry blocks were manufactured with six half-bricks joined by five 10 mm-thick mortar layers (Fig. 1a). The nominal dimensions of the blocks were 125 mm × 120 mm × 380 mm.

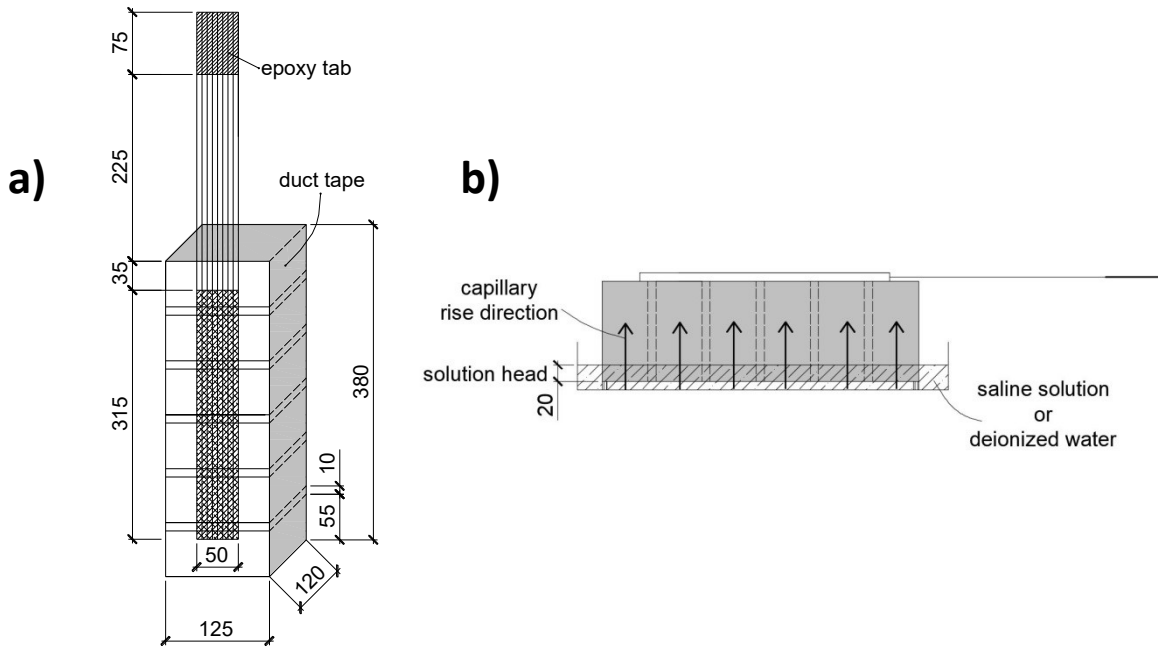


Fig. 1. a) Geometry of the steel FRCM-masonry joints and b) capillary rise direction of the saline solution (mixture of sodium chloride and sodium sulfate) or deionized water. Dimensions in mm.

The bricks used were commercially available solid fired-clay bricks with the following dimensions 55 mm × 120 mm × 250 mm. Twenty cylinders of nominal dimensions equal to 50 mm (diameter) × 50 mm (length) were cored from five bricks. Out of twenty cylinders, seven were used to determine the tensile strength of bricks, through splitting tests, while thirteen were used to obtain the compressive strength of bricks, according to EN 772–1 [25]. The tensile and compressive strengths of bricks resulted equal to 3.16 MPa (CoV=12%) and 20.3 MPa (CoV=17%), respectively. The mortar employed for the joints was a dry-mix commercially available mortar, based on natural hydraulic lime (NHL 3.5) and classified as M5 according to EN 998-2 [26], as reported in the manufacturer’s data sheet [27]. The amount of water recommended by the manufacturer (17.6 wt.%) was used to mix the mortar. Three 40 mm × 40 mm × 160 mm prisms of mortar were cast, in order to determine its flexural and compressive strengths after they were cured for 28 days according to EN 1015–11 [28]. The flexural and compressive strengths resulted equal to 2.8 MPa (CoV=4.8%) and 12.7 MPa (CoV=5.3%), respectively.

After the masonry blocks were cured in laboratory conditions for one month, steel FRCM strips were applied to one face of 15 blocks (Fig. 1a). Prior to applying the FRCM strips, blocks were soaked in water for



45 minutes to prevent the depletion of water from the composite grout. The application of the composite was carried out using the materials and the steps below:

- A layer (thickness 4 mm, width 50 mm, length 315 mm) of mortar was applied to the bonded area of one block surface. The thickness of the layer of mortar was 4 mm as per the manufacturer's recommendation. A commercially available dry-mix natural hydraulic lime-based mortar (NHL 3.5) with quartz sand, class M15 according to EN 998-2 [26], was used. Its flexural and compressive strengths were determined on three prisms cast from the same batch (40 mm × 40 mm × 160 mm) according to EN 1015–11 [28] after they were cured for 28 days, and resulted equal to 4.7 MPa (CoV=0.14%) and 13.5 MPa (CoV=3.7%), respectively. The mortar used for the composite is referred to as 'matrix' in the remainder of the paper to avoid confusion with the mortar used for the joints;
- A steel fiber sheet (width 50 mm, length 635 mm) consisting in a unidirectional sheet made of ultra-high strength galvanized steel cords, fixed to a secondary 6 mm-spaced fiberglass micromesh, was applied and delicately pressed into the first matrix layer. The cross-sectional area of the cords, equivalent thickness, and number of cords per unit width of the sheet are equal to 0.538 mm<sup>2</sup>, 0.084 mm and 0.157/mm, respectively. According to the manufacturer's data sheet [29], the tensile strength, ultimate strain, and modulus of elasticity of the steel fibers are 3000 MPa, 2%, and 190 GPa, respectively. Fibers were left bare outside the bonded area for a length equal to 335 mm;
- A second 4 mm-thick layer of matrix was applied onto the steel fiber sheet. The total thickness of the FRCM composites resulted equal to 8 mm.

The final configuration of the steel FRCM-masonry joints is reported in Fig. 1a.

All the FRCM-masonry joints were cured under a wet cloth at room temperature in the laboratory, so in moist conditions, in order to avoid a premature water evaporation from the matrix and allow an almost complete hardening of the composite. For this reason, a curing time of 1 month was considered adequate for the mortar selected. It is noteworthy that the materials used in the present study (bricks, mortar joints and FRCM system), as well as the dimensions of the masonry joints were the same adopted in [24], for the sake of comparison.

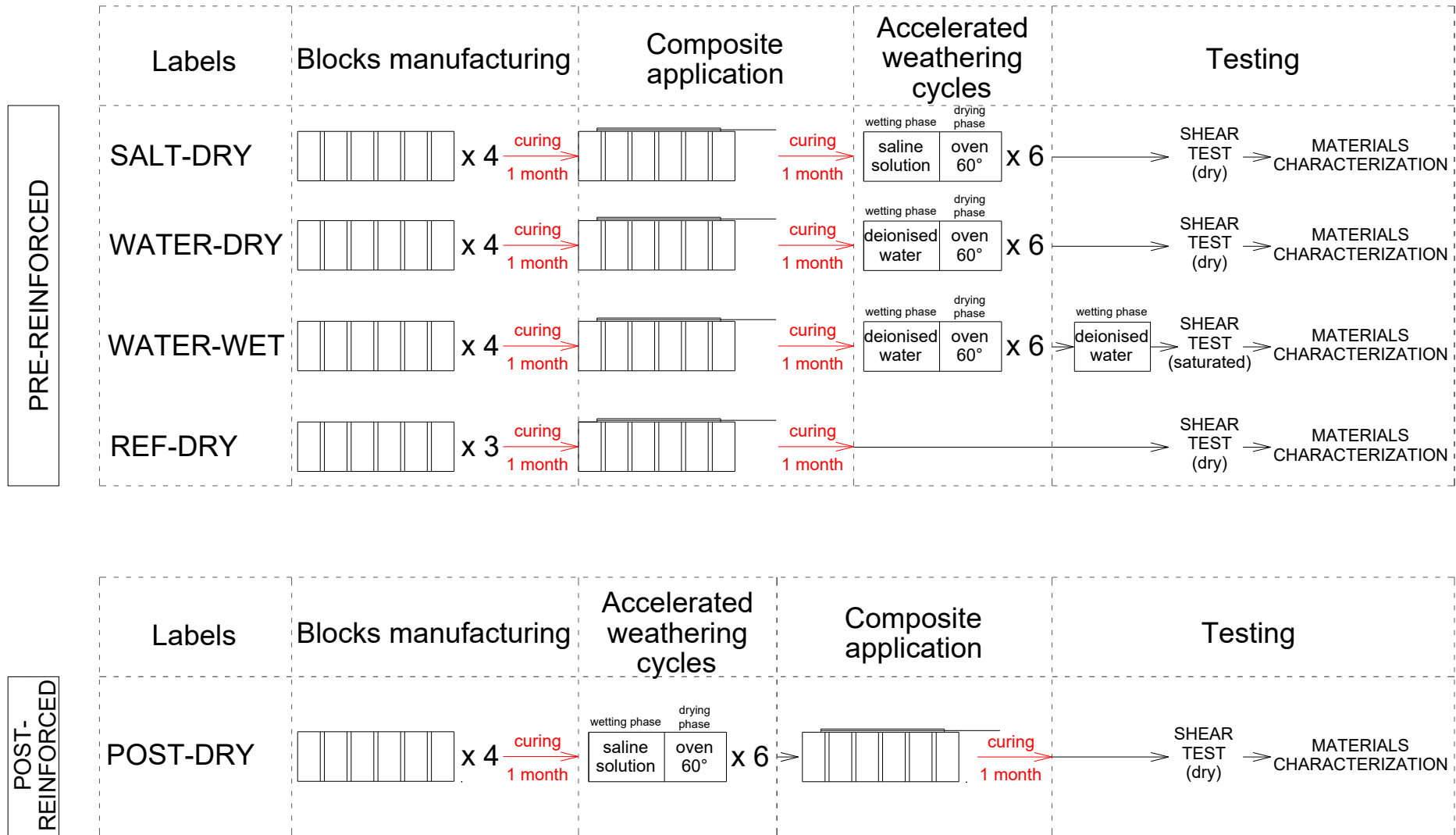


Fig. 2. Scheme of the FRCM-masonry joint labels, construction, composite application, weathering cycles, and material testing.

### 3.2. Accelerated weathering method

On the basis of past experimental results published by the authors [30, 31], two types of weathering conditions were selected, namely six wetting-drying cycles in saline solution or in deionized water. In all the FRCM-masonry joints, a duct tape was applied to the four lateral faces of the specimens (Fig. 1a), in order to make evaporation occur through the top surface (the one to which the composite was applied). The configuration with total wrapping [24] was dismissed, as no meaningful differences in the results were found with respect to the partial wrapping configuration.

Figure 2 shows a scheme of the specimen labels, construction, composite application, conditioning procedures, as well all testing conditions.

The first type of cycles comprised a wetting phase in a saline solution followed by a drying phase. In the wetting phase, the specimens were partially immersed in an aqueous solution at lab temperature ( $20^{\circ}\text{C}\pm 2^{\circ}\text{C}$ ) of sodium chloride, NaCl (2 wt%), and sodium sulfate decahydrate,  $\text{Na}_2\text{SO}_4\cdot 10\text{H}_2\text{O}$  (8 wt%) (Fig. 1b), with a solution head of 20 mm. Based on preliminary tests, two days were considered sufficient to obtain a reasonably complete saturation of the specimens. The wetting phase was followed by a drying phase in a ventilated oven at  $60^{\circ}\text{C}$  for three days. In three days, the specimens did not completely dry out, but only a small amount of residual moisture was present and it was considered too low to hinder the absorption of water in the following wetting phase. The duration of the wetting and drying phases (two and three days, respectively) was chosen to compromise between the attainment of the desired saturation/drying level and the need of a reasonable test duration. Those specimens that were subjected to six cycles in the saline solution are named 'SALT-' (4 specimens).

This procedure is different from several points of view from the main standard tests on the resistance of porous materials to salt crystallization, i.e. EN 12370 [32], RILEM MS-A.1 [33], and RILEM MS-A.2 [34].

These standards suggest the use of highly aggressive saline solutions (14 wt% sodium sulfate in EN 12370 [32], 10 wt% sodium sulfate and 10 wt% sodium chloride in RILEM MS-A.1 [33] and saturated sodium sulfate solution in RILEM MS-A.2 [34]) and in some cases also highly aggressive cycles (e.g., total immersion followed by oven drying at  $105^{\circ}\text{C}$  in EN 12370 [32]). Therefore, the accelerated weathering leads to the

failure of the materials in a number of cycles that depends on the material under testing and is not reported in the standards (only EN 12370 [32] indicates a maximum number of 15 cycles, but also adds that failure may occur in fewer cycles). No relationship between the number of cycles and the number of years of real exposure conditions is given in the standards and EN 12370 [32] clearly states that it aims at assessing the *relative resistance* of stone to salts. In this work, the aim is not to perform *extreme* salt crystallization cycles that could lead to a severe damage of the FRCM composite to the point that its adhesion to the substrate is compromised. The accelerated weathering protocol was designed to reproduce, in a relatively short period of time, damaging salt crystallization cycles and achieve realistic concentrations of salts in the masonry joints, i.e. amounts that can be found in real historical buildings [35, 36]. Thus, a lower concentration of salts with respect to the amount suggested in the standards (2 wt% sodium chloride and 8 wt% sodium sulfate decahydrate) and a lower temperature for oven drying (60 °C) were selected.

The second type of cycles comprised a wetting phase in deionized water and a drying phase in oven, Fig. 2. The specimens were partially immersed in deionized water (water head 20 mm) at lab temperature (20°C±2°C) for two days. The wetting phase was followed by a drying phase in a ventilated oven at 60°C for three days. The specimens that were subjected to six cycles in water are labelled 'WATER-' (8 specimens). As it was mentioned in Section 2, the cycles in water resulted essential to detect a possible enhancement of the matrix curing, which in turn allowed to separate the effect of water from the effect of salts. In fact, the alternation of water imbibition and moderately high temperature may alter the mechanical properties of the matrix by enhancing its curing [24].

In addition to the specimens described above, in four masonry blocks the composite was not applied and the blocks were subjected to the same cycles in saline solution carried out for SALT- specimens. After six cycles, the efflorescence and the crumbling fragments present on the top surface of the blocks were removed using a steel brush. Subsequently, the steel FRCM composite was applied and cured, following the same procedure described in Section 3.1 for the other specimens, Fig. 2. This set of FRCM-masonry joints, named 'POST-', was used to investigate the bond capacity of the FRCM composites when applied to an

already weathered surface, i.e. to a salt-damaged masonry. In fact, FRCM composites are often employed to strength historical masonry that has been exposed during its lifetime to different weathering processes, which possibly led to salt accumulation.

Finally, an additional aspect was studied in the present campaign. In order to determine if the presence of moisture in the pores of the specimens (masonry and composite) may affect the FRCM-substrate bond behavior, four out of the eight WATER- specimens were tested using the single-lap set-up immediately after the cycles were completed, i.e. in dry conditions (labelled 'WATER-DRY'), while the other four were immersed in water after the cycles, until constant weight was reached, and finally tested, i.e. they were tested in saturated conditions (labelled 'WATER-WET'). The role of moisture on the bond capacity was considered worth of investigation, as highlighted in previous studies [37-39]. The suffix '-DRY' was added to all specimens that were tested in dry conditions.

Three steel FRCM-masonry joints (labeled 'REF-DRY') were considered as control specimens and not subjected to any conditioning.

### **3.3. Direct shear test**

As illustrated in Fig. 2, at the end of the accelerated weathering cycles, all specimens were subjected to direct shear tests, specifically single-lap shear tests. In Fig. 3, a photo of an FRCM-masonry joint at the beginning of the test is shown. For the sake of brevity, the experimental set-up will not be reported herein, as a complete description of the test configuration is available in [24,40-42]. The main features of the set-up and testing procedure are briefly summarized below:

- A tensile force was applied to the composite strip, which was gripped through a 75 mm-long epoxy tab by the head of a 100 kN capacity servo-hydraulic universal testing machine;
- The FRCM-masonry joints were restrained between two thick steel plates connected by four instrumented threaded rods;
- Two vertical LVDTs (linear variable displacement transformers) were employed to measure the relative displacement between the composite strip (close to the top edge of the bonded area) and

the adjacent masonry surface. The displacements measured by the LVDTs are indicated as  $g_a$  and  $g_b$ . The global slip  $g$  is the average of these two measurements;

- Two horizontal LVDTs were applied in the back of the specimen and reacted off the face of the block opposite to the surface where the composite was applied in order to monitor the out-of-plane displacement and/or rotations of the specimen during the test due to the eccentricity of the applied load [43];
- All tests were conducted at a constant global slip rate equal to  $0.84 \mu\text{m/s}$  until failure.

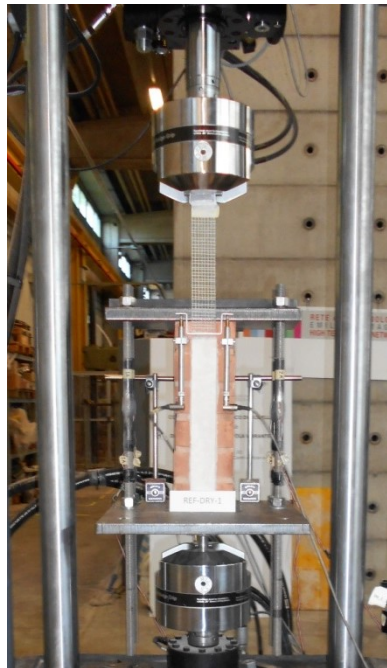


Fig. 3. Experimental test set-up: FRCM-masonry joint at the beginning of the direct shear test. Two vertical LVDTs are employed to measure the relative displacement between the composite strip and the adjacent masonry surface.

#### **3.4. Materials characterization: salt distribution and material porosity**

After the direct shear tests were performed, samples of material were collected by chisel fragmentation from each type of specimen (REF-DRY, WATER-DRY, WATER-WET, SALT-DRY and POST-DRY).

Firstly, the distribution of chloride and sulfate in the specimen was investigated by taking fragments from four different locations in the masonry blocks, Fig. 4: two locations were in the brick and two in the matrix, since the mortar joints are expected to play a minor role in the salt distribution [24]. In particular, brick samples were taken just beneath the top surface at two locations (labelled B-L and B-C as in Fig. 4) that

correspond, respectively, to the center and edge of the FRCM strip. The locations were chosen to investigate if the composite might have caused an undesired accumulation of salts in the brick region beneath the composite itself, which could possibly lead to the composite detachment. Moreover, samples of the composite matrix were collected from the internal layer of the matrix, i.e. underneath the fibers (M-C-INT), and from the external layer, i.e. above the fibers (M-C-EXT), in order to check if the steel fiber sheet itself created a barrier to the capillary flow of the saline solution. All the fragments were collected far from the edges. Particular care was used to remove the surface efflorescence, when present.

Soluble salts, in terms of anions, were determined on the fragments by grinding to powder (<0.075 mm), extraction with deionized boiling water (electrical conductivity <0.02  $\mu$ S), filtration by blue ribbon filter, and final ion chromatography, IC (in a Dionex ICS-1000, equipped with Ion Pac AG14A guard column and Ion Pac AS14A inorganic anion-exchange column kept at 30 °C; measuring cell temperature 35 °C). Results are the average of two samples for each location. To obtain a representative result, these two samples were extracted from two different FRCM-masonry joints for each type of specimen.

Mercury intrusion porosimetry, MIP (Porosimeter 2000 with a Fisons Macropore Unit 120) was carried out to investigate the effect of salt crystallization cycles, in terms of salts accumulation and formation of micro-cracks in the materials after the cycles. In particular, since the failure of the specimens occurred inside the composite (at the interface between the fibers and the matrix), MIP was conducted on matrix samples collected from the location M-C-EXT reported in Fig. 4. For the samples extracted from SALT-DRY specimens, MIP was carried out also after the removal of the salts (desalination) by poultice, using a mix of deionized water and cellulose pulp and applying it all around the fragment after the application of a sheet of Japanese paper.

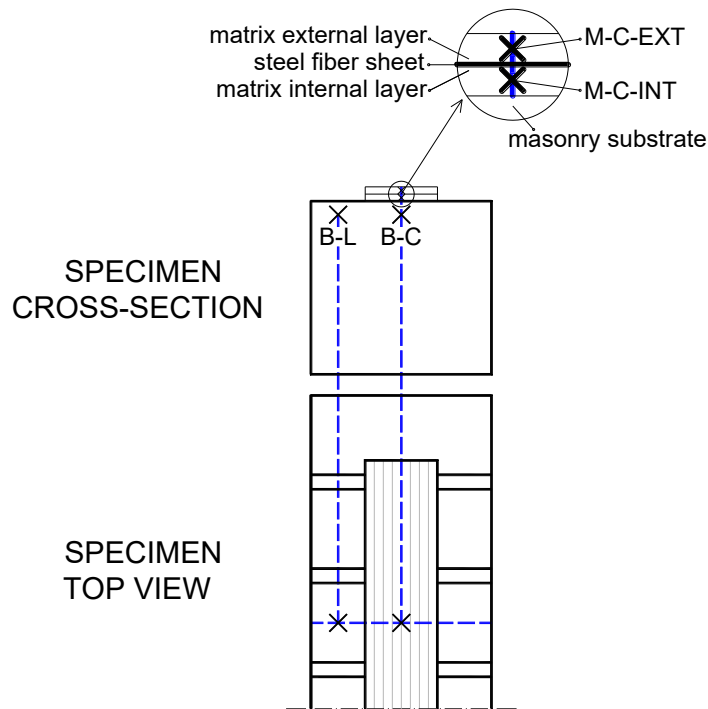


Fig. 4. Sampling location for material characterization (M = matrix, B = brick, L = lateral sampling location, C = central sampling location, EXT = external layer, INT = internal layer).

#### 4. Results and discussion

##### 4.1. Visual observation of the FRCM-masonry joints before the direct shear test

Figure 5 shows some selected specimens at the end of the conditioning procedure (6<sup>th</sup> cycle). Images of the WATER-WET specimens are not reported, for the sake of brevity, since they were subjected to the same cycles of the WATER-DRY specimens. WATER-DRY specimens, Fig. 5a and b, exhibit a slight formation of whitish efflorescence on the surface of the composite, while no efflorescence is visible on the bricks and a negligible amount on the mortar joints. The formation of such efflorescence has to be ascribed to salts that were already present in the original materials of the blocks and of the composite matrix, solubilized by water and transported by the capillary flow up to the top surface of the specimens.

As expected, the efflorescence formation is much more evident in the SALT-DRY specimens (Fig. 5c and d). The whitish salts layer is thicker and more continuous and, interestingly, its formation is not uniformly distributed over the top surface, but rather salts accumulated in the central part of the specimens, near and on top of the composite (Fig. 5c). This non-uniform distribution suggests that the paths, which the saline solution followed during its capillary rise from the bottom to the top of the specimens, were not



uniform due to the presence of the strip. This phenomenon is confirmed by the efflorescence observed on the POST-DRY specimens at the end of the 6<sup>th</sup> cycle, before the composite was applied (Fig. 5e and f). When the composite is not present, efflorescence is clearly distributed over the entire top surface of the block and no preferential paths were followed by the capillary rise, hence evaporation and salt precipitation occurred uniformly over the surface. In Fig. 6a, the POST-DRY specimens after the removal of the superficial efflorescence with a steel brush and before the application of the composite are shown.

A completely different efflorescence distribution with respect to SALT-DRY specimens was observed in the POST-DRY specimens (Fig. 6b and c) in which the cycles were performed, then the composite was applied and cured for one month, and finally the shear test was carried out. In fact, efflorescence is distributed over the entire top surface, hence not only in the central part near and on top of the composite as in the SALT-DRY specimens (Fig. 5c and d). The curing of the composite in moist conditions (under a wet cloth), which was necessary to achieve the development of the mortar strength, seems to have caused the dissolution of the salts in the masonry blocks and their transport towards the top surface during the final drying; in this way also the composite exhibited a marked salts accumulation.

It should be noted that for all specimens that underwent the cycles in saline solution (SALT-DRY and POST-DRY), some flaking of the bricks was visually observed, but no detachment or powdering of the composite was visible.

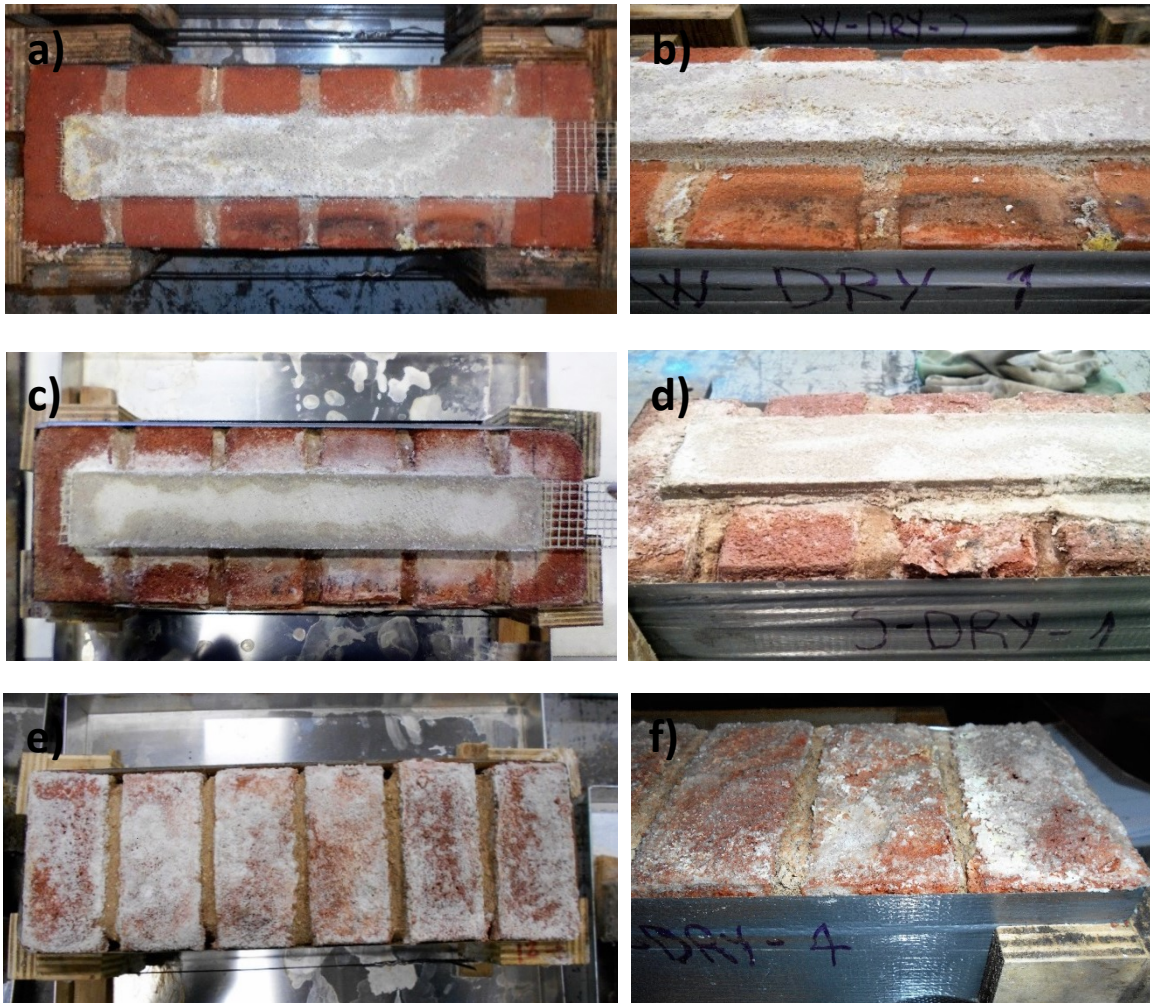


Fig. 5. Photos of selected WATER-DRY (a,b), SALT-DRY (c,d), and POST-DRY (e,f) specimens at the end of the conditioning procedure (6<sup>th</sup> cycle) and before the shear test was performed.



Fig. 6. Photos of selected POST-DRY specimens: a) at the end of the conditioning procedure and after removal of the superficial efflorescence with a metal brush; b) and c) after curing of the composite and before the shear test.

#### 4.2. Direct shear test

Results from the direct shear test are collected in Fig. 7. Global slip  $g$ , as the average of the two measurements,  $g_a$  and  $g_b$ , recorded during the test by the two vertical LVDTs is reported in the horizontal axis, while the applied load  $P$  measured by the load cell of the testing machine is plotted in the vertical axis. In Table 1, a summary of the results for all specimens is reported.

A frequent failure mode of the single-lap shear tests was interlaminar debonding, i.e. the fibers slipped with respect to the matrix. As the slippage of the fibers progressed, the matrix was damaged and eventually separation between the internal and external layers of matrix occurred. The internal layer of matrix remained attached to the substrate (failure mode A in Fig. 8 and Table 1) [44], while the external layer detached and the fibers in some cases remained bonded to the external layer, while in other cases the

external layer detached from the fibers. Additional failure modes were observed and are classified in Fig. 8. In particular, REF-DRY specimens showed a type B failure mode: i.e. the slippage of the fibers occurred, however a portion of the internal layer of the matrix detached from the substrate. Type C failure mode (i.e. debonding of the FRCM strip from the masonry substrate) occurred for one specimen, as listed in Table 1. It should be noted that debonding with cohesive fracture of the support, which is a typical failure mode for FRP composites, was not observed for any specimen. For sake of completeness, it should be noted that in other experimental campaigns dealing with direct shear tests on steel FRCM-masonry joints that employed the same materials, an additional failure mode was observed, i.e. the rupture of the fibers [40]. However, this type of failure did not occur for any of the specimens of the experimental campaign herein presented. The differences in failure modes are reflected in different applied load-global slip curves. In fact, the response of direct shear tests cannot be represented by a single curve, but rather by four types of response (type 1, 2, 3 and 4, Fig. 7a).

All curves show an almost linear behavior at low load values. For increasing load values, a non-linear behavior follows, which corresponds to the formation of micro-cracks in the matrix (Fig. 7a). After the linear part, the behavior of the specimens depends on several factors as described below.

The first type of curve (type 1 in Fig. 7a) is characterized by a load drop followed by an almost-horizontal branch until the end of the test. The load drop corresponds to the coalescence of the micro-cracks into a macro-crack at the interface between the two layers of matrix. The propagation of the macro-crack at the interface occurred at an almost constant load. This behavior can be identified for specimens REF-DRY-1, REF-DRY-2 (Fig. 7b), WATER-DRY-1, WATER-DRY-3, all SALT-DRY specimens, and POST-DRY-2 specimen. The global slip range ( $g_1, g_2$ ) that defines the horizontal part of the curve, corresponds to the progression of the interfacial macro-crack towards the free-end of the composite (i.e., the end of the bonded area opposite to where the load was applied). The constant load, which is calculated as the average load between  $g_1$  and  $g_2$ , is indicated as  $\bar{P}$  and represents the debonding load, bond capacity, or load-carrying capacity.  $\bar{P}$  is reported in Table 1 for each specimen together with its average  $\bar{P}_{avg}$  for each group. Type 1 curve might feature an

ascending tail that corresponds to the end of the test, which might be characterized by a dominant fracture mechanics Mode-I condition. The tail is always disregarded in the calculations.

The failure modes that are associated with type 1 curve were the interlaminar failure mode (failure mode A) or the mixed failure mode (failure mode B).

A second type of curve (type 2 in Fig. 7a) is the one where the load drop is not detectable, since the load reaches smoothly an almost constant value after the linear part, i.e. without any significant drop. Specimen REF-DRY-3, all WATER-WET specimens, and specimens POST-DRY-1, POST-DRY-3, and POST-DRY-4 are characterized by this type of curve. These specimens exhibited either an interlaminar failure mode or a mixed one (failure modes A or B). In this case, the selection of the interval  $g_1 - g_2$  to define  $\bar{P}$  is done by identifying the almost-horizontal part on the curve.

The type 3 curve in Fig. 7a is characterized by one or more load drops, but no nominally constant load branch (plateau) can be identified. Specimen WATER-DRY-4, for which the failure is characterized by a sudden detachment at the composite-to-substrate interface (failure mode C), exhibited a type 3 response. In this case, the debonding load  $\bar{P}$  is not defined since the  $g_1 - g_2$  interval where the load is constant cannot be identified.

The last type of curve (type 4 in Fig. 7a) is characterized by an initial linear portion followed by an always ascending non-linear branch until failure that occurs when the fibers rupture. As stated before, this failure mode was not observed in any of the specimens tested.

The debonding load, when calculated, depends on how the  $g_1 - g_2$  interval is chosen. However, it should be noted that even if the global slip interval  $g_1 - g_2$  is selected on the graph, slight variations of the values of  $g_1$  and  $g_2$  do not affect significantly the corresponding debonding load values [40].

Additionally, for each specimen, the peak load  $P^*$ , its average value for each group of specimens  $P_{avg}^*$ , as well as the values of  $g_1$  and  $g_2$  are reported in Table 1. Parameters  $\Delta^*$  and  $\bar{\Delta}$  in Table 1 are defined as:

$$\Delta^* = \frac{P_{avg}^*(COND) - P_{avg}^*(REF)}{P_{avg}^*(REF)} 100\%; \quad \bar{\Delta} = \frac{\bar{P}_{avg}(COND) - \bar{P}_{avg}(REF)}{\bar{P}_{avg}(REF)} 100\%$$

where  $P_{avg}^*(COND)$  and  $\bar{P}_{avg}(COND)$  are average peak load and average load-carrying capacity of the conditioned specimens, respectively, while  $P_{avg}^*(REF)$  and  $\bar{P}_{avg}(REF)$  are the average peak load and average load-carrying capacity of the reference specimens, respectively.

The results of the direct shear test for the FRCM-masonry joints that cycled in water and were tested in dry conditions (WATER-DRY) are collected in Fig. 7c. Only three curves are reported: the curve relative to WATER-DRY-2 specimen was disregarded since an anomalous rotation of the specimen was noted during the test. In general, the responses show a behavior similar to the control specimens (REF-DRY). A comparison between the results of REF-DRY and WATER-DRY specimens in Table 1, indicates that the average peak load  $P_{avg}^*$  and average bond load  $\bar{P}_{avg}$  of WATER-DRY specimens show a decrease with respect to REF-DRY values (about 12% and 22%, respectively). These values appear to confirm past experimental results [24]. The wetting/drying cycles in deionized water/oven did not cause any increment in the load-carrying capacity of the WATER-DRY specimens. In fact, the FRCM-masonry joints were left to cure under a wet cloth for one month, which assured an almost complete hydration of the hydraulic fraction of the binder, hence no additional mechanical benefit was achieved by the cycles in water. The slight decrease exhibited by WATER-DRY specimens with respect to REF-DRY specimens might be ascribed to some limited spots of corrosion detected in the steel cords (see Section 4.3). However, a high coefficient of variation characterizes the results of the WATER-DRY specimens, since only the results of two specimens were used to compute the average of the load-carrying capacity. Additional tests are necessary to confirm the present results.

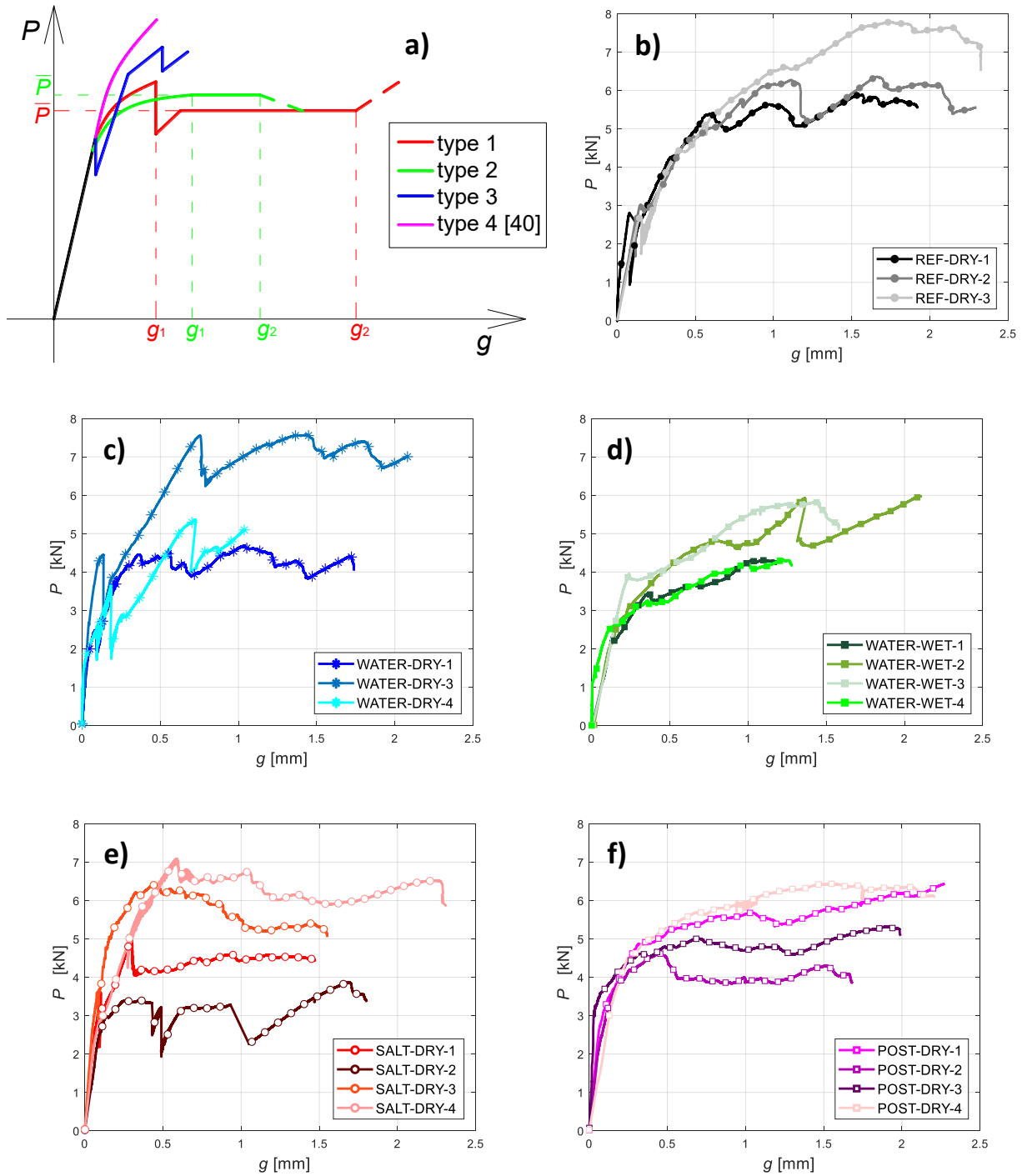


Fig. 7. a) Idealized applied load-global slip responses for FRCM-masonry joints, b) applied load-global slip curves of REF-DRY, c) applied load-global slip curves of WATER-DRY, d) applied load-global slip curves of WATER-WET, e) applied load-global slip curves of SALT-DRY, and f) applied load-global slip curves of POST-DRY specimens.

Table 1. Direct shear test results<sup>(1)</sup>. Coefficient of variation within parentheses.

Specimen	$P^*$	$P_{avg}^*$	$\Delta^*$	$\bar{P}$	$\bar{P}_{avg}$	$\bar{\Delta}$	$g_1$	$g_2$	✓ or ×	FAILURE MODE	CURVE TYPE	
	[kN]	[kN]	[%]	[kN]	[kN]	[%]	[mm]	[mm]				
REF-DRY-1	5.88	6.7 (14.9)		5.33	6.2 (19.6)		0.710	1.742	✓	B	1	
REF-DRY-2	6.36			5.61			1.224	2.081	✓	B	1	
REF-DRY-3	7.79			7.56			1.514	2.165	✓	B	2	
WATER-DRY-1	4.69	5.9 (25.7)	-12.0	3.96	5.2 (34.0)	-21.8	0.603	1.453	✓	B	1	
WATER-DRY-2	×			×			×	×	×	×	×	×
WATER-DRY-3	7.57			6.48			0.788	1.924	✓	B	1	
WATER-DRY-4	5.36			n.d. <sup>(2)</sup>			n.d. <sup>(2)</sup>	n.d. <sup>(2)</sup>	✓	C	3	
WATER-WET-1	4.31	5.1 (18.0)	-23.5	4.27	4.7 (14.4)	-29.6	1.001	1.169	✓	B	2	
WATER-WET-2	5.98			4.67			0.922	1.419	✓	B	2	
WATER-WET-3	5.82			5.63			1.059	1.471	✓	A	2	
WATER-WET-4	4.31			4.24			0.970	1.238	✓	B	2	
SALT-DRY-1	4.98	5.6 (25.9)	-16.3	4.27	4.8 (30.2)	-27.5	0.316	1.458	✓	B	1	
SALT-DRY-2	3.86			3.18			0.431	1.692	✓	A	1	
SALT-DRY-3	6.41			5.31			1.019	1.508	✓	B	1	
SALT-DRY-4	7.09			6.61			0.616	2.277	✓	A	1	
POST-DRY-1	6.43	5.7 (15.6)	-14.6	5.83	5.3 (19.1)	-20.3	0.798	2.063	✓	A	2	
POST-DRY-2	4.62			4.01			0.563	1.597	✓	A	1	
POST-DRY-3	5.32			5.09			0.742	1.982	✓	A	2	
POST-DRY-4	6.44			6.35			1.297	2.070	✓	A	2	

<sup>(1)</sup> Note that results of specimens marked with × were not considered in the calculation of average values (indicated by subscript *avg*)

<sup>(2)</sup> n.d. = value not defined

In Fig. 7d, the  $P$ - $g$  curves related to the specimens that cycled in water and were tested in saturated conditions (WATER-WET) are represented. It is well known that the presence of water inside the pores of the materials causes additional pressures, which is detrimental for the mechanical properties [38]. In fact, considering the average peak load  $P_{avg}^*$  and parameter  $\Delta^*$  in Table 1, WATER-WET specimens exhibit the



lowest average peak load. In particular, a 23% decrease is observed with respect to REF-DRY specimens. In addition, the average debonding load  $\bar{P}_{avg}$  was 30% lower than the average capacity of REF-DRY specimens. Figure 7e reports the response of specimens that cycled in saline solution and were tested in dry conditions (SALT-DRY). The average peak load  $P_{avg}^*$  and bond capacity  $\bar{P}_{avg}$  show a decrease with respect to the average values of REF-DRY specimens of 16% ( $\Delta^*$ ) and 27% ( $\bar{\Delta}$ ), respectively.

This result appears to conflict with the results obtained in the previous experimental campaign conducted by the authors in [24], in which an improvement of the bond properties was reported for specimens that cycled in saline solution. However, it should be noted that the FRCM-masonry joints in [24] were subjected to a smaller number of crystallization cycles with respect to the present research (4 rather than 6) and, moreover, sodium sulfate alone was used for the saline solution [24], rather than a mix of sodium sulfate and sodium chloride as it was employed in the present study. Thus, it is reasonable to state that the additional cycles and the addition of sodium chloride to the saline solution led to a decrease of the interfacial bond capacity. Further details to interpret this result are illustrated in the next sections, especially in terms of presence of corrosion due to chloride.

It is interesting to note that the average peak value  $P_{avg}^*$  of POST-DRY specimens is comparable to that of SALT-DRY specimens (5.7 kN for POST-DRY and 5.6 kN for SALT-DRY in Table 1). While, the average load-carrying capacity  $\bar{P}_{avg}$  is slightly higher for POST-DRY specimens with respect to SALT-DRY specimens (Fig. 7f and Table 1). This is a preliminary result, since to the authors' knowledge, no literature studies are available on the bond behavior of FRCM composites applied to already salt contaminated masonry structures. From the present study, it can be inferred that the load-carrying capacity of FRCM composites applied to masonry blocks prior to being subjected to accelerated weathering cycles is similar to that of FRCM composites applied to masonry blocks that before the application underwent conditioning cycles. However, further research must be undertaken to confirm the present experimental result.

It should be observed that, as expected for this class of materials, a high coefficient of variation characterizes the results of the tests. The high variability is related to several aspects: masonry is a material that has a significant amount of built-in variability, the use of an inorganic matrix, which is a lime-based

mortar, adds variability since its behavior is strongly dependent on the casting conditions, curing conditions, and on the weathering conditions for this specific study. For example, during the dry phase, the temperature inside the oven may be non-uniformly distributed around the specimens even if the oven is ventilated. Temperature gradients might have modified locally the physical/mechanical properties of the matrix even within the same specimen. The presence of spots of corrosion along the fibers represents a further variable, since their distribution is random along the fiber sheet. Therefore, additional tests are necessary to confirm the present experimental results and to increase the experimental database on the topic, which is still extremely limited.

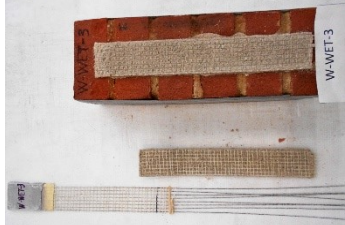


Label	Description	Photo
A	Interlaminar failure mode: slippage of the fibers from the internal layer of matrix that remained attached the substrate	
B	Mixed interlaminar failure mode: slippage of the fibers from the internal layer of matrix, of which only a portion remained attached to the substrate	
C	Fracture surface at the substrate/internal layer of the matrix interface: the internal layer of the matrix detached from the substrate	

Fig. 8. Failure modes of the specimens in the direct shear test.

#### 4.3. Visual observation of the FRCM-masonry joints after the direct shear test

The visual observation of the SALT-DRY and POST-DRY specimens after the single-lap test was performed (Fig. 9a and b, respectively) revealed that some corrosion occurred on the surface of the galvanized steel cords. The corrosion is related to the presence of sodium chloride in the solution employed in the wetting cycles, as no corrosion was observed when only sodium sulfate was used [24]. Some spots of corrosion were observed also in the WATER-series specimens, although very limited.

To the authors' best knowledge, the corrosion behavior of galvanized steel elements embedded in mortars (FRCM, renders, grouts etc.) has not been investigated so far, while several research works addressed the corrosion of galvanized steel reinforcement in concrete [45-47]. Although reinforced concrete is different from FRCM, some useful information can be taken from relevant papers, in the absence of more specific studies. The use of galvanized steel rods in concrete was proposed as a preventive measure for corrosion control in reinforced concrete structures exposed to carbonation, by exploitation of the zinc passivation process [48]. Compared to ordinary reinforcement, galvanized bars lengthen also the service life of structures exposed to chlorides, but the galvanized steel passivity is lost once chloride content in the concrete exceeds a threshold concentration which is reported to be 2 wt.% [49], hence galvanized bars are suitable only for concrete with mild chlorides contamination [48]. This limitation also led to the development of inhibitors for galvanized steel reinforcement [49]. However, some authors highlighted that the effect of chloride ions on the corrosion resistance of galvanized steel is strongly affected by concrete carbonation [48]. In particular, these authors exposed concrete specimens with galvanized reinforcements to wet-dry cycles in tap water and in a 3.5% NaCl solution at room temperature and found that carbonation changes the nature of the passivating layer (from calcium hydroxyzincate to amorphous  $ZnCO_3$  and  $Zn_5(CO_3)_2(OH)_6$ ). The new layer still has passivating properties towards wet-dry cycles in tap water, but is susceptible to chloride attack by formation of zinc hydroxychloride on the surface. As a result, corrosion may occur in carbonated concrete at markedly lower chlorides amounts (0.29 wt.%) than those indicated in the literature for galvanized steel embedded in non-carbonated concrete (2 wt.%).

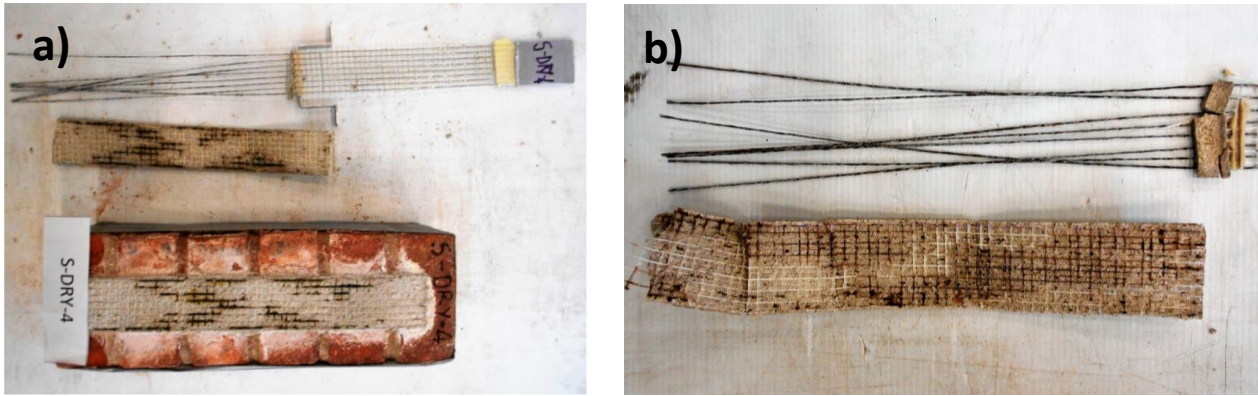


Fig. 9. Presence of corrosion in a) SALT-DRY and b) POST-DRY specimens after the single-lap shear test was performed.

Based on these experimental results found for concrete, some susceptibility of the galvanized steel cords to chloride corrosion can be expected also in the FRCM matrix, although this aspect deserves further investigation. In fact, the matrix investigated in the present study is different from concrete in terms of binder (natural hydraulic lime rather than portland cement), microstructure (much more porous than ordinary concrete), and carbonation rate. In particular, the evolution of pH due to carbonation is a very complex phenomenon, as it depends on several parameters, such as porosity and microstructure, binder chemistry, environment, moisture content, and pore solution chemistry. Another aspect that deserves further investigation is the fact that the drying phase of the cycles is performed at a temperature equal to 60 °C, which differs from literature studies on galvanized steel (carried out by wetting-drying cycles at room temperature [48-50]). Hence, the role of temperature should be investigated. In fact, in galvanized steel exposed to atmosphere, temperature has opposite effects, as it accelerates electrochemical reactions, but at the same time accelerates the evaporation of the humidity deposited on the metal, decreasing the time of wetness for the metal surface [51].

#### 4.4. Materials characterization

##### 4.4.1. Salts amount and distribution

Results from IC are collected and summarized in Table 2. The sampling locations are described in Fig. 4. REF-DRY samples are taken as representative of the original materials, as they were subjected to no

weathering cycles. Slight amounts of sulfate and chloride anions are present both in the bricks and the composite matrix (higher in the latter one), a common occurrence for these types of building materials [30,35,36].

Table 2. Salt content of matrix and brick samples extracted from REF-DRY, WATER-DRY, WATER-WET, SALT-DRY and POST-DRY specimens.

Samples	Sampling locations (as in Fig. 4)	Chloride anions (Cl <sup>-</sup> , wt%)	Sulfate anions (SO <sub>4</sub> <sup>2-</sup> , wt%)	Total anions (wt%)
REF-DRY	B-L	0.098	0.103	0.121
	B-C	0.105	0.062	0.120
	M-C-INT	0.118	0.558	0.615
	M-C-EXT	0.078	0.525	0.657
WATER-DRY	B-L	0.106	0.147	0.253
	B-C	0.104	0.076	0.180
	M-C-INT	0.146	0.817	0.963
	M-C-EXT	0.171	0.719	0.890
WATER-WET	B-L	0.122	0.595	0.717
	B-C	0.119	0.289	0.408
	M-C-INT	0.142	0.562	0.704
	M-C-EXT	0.104	0.102	0.206
SALT-DRY	B-L	0.712	1.831	2.543
	B-C	0.682	1.034	1.716
	M-C-INT	1.025	2.927	3.952
	M-C-EXT	1.045	2.286	3.331
POST-DRY	B-L	1.052	0.765	1.816
	B-C	0.726	0.473	1.199
	M-C-INT	1.163	1.868	3.031
	M-C-EXT	1.384	1.243	2.627

When compared with REF-DRY samples, WATER-DRY and WATER-WET samples (that underwent cycles in deionized water), exhibited an increase of the anions amount. This difference is due to the washout of the salts by the capillary water flow and to their accumulation in the upper part of the FRCM-masonry joints. For WATER-DRY and WATER-WET samples, the fact that efflorescence are present mostly over the composite is due to the higher initial content of salts in the matrix with respect to bricks. Salts in the bricks, determined by IC, appear to be higher in the lateral location (B-L) than in the central location beneath the composite (B-C). This seems to confirm the hypothesis that the water flow follows the most permeable path, i.e. the masonry surrounding the composite strip.

As expected, the anions amount strongly increases in those specimens that underwent cycles in the saline solution (SALT-DRY). In particular, the composite matrix exhibits an average  $\text{Cl}^-$  amount equal to 1.0% and an average  $\text{SO}_4^{2-}$  amount equal to 2.6%. Although a low number of weathering cycles were carried out (six), these percentages are high and comparable to the amount of sulfates and chlorides that can be found in real historical buildings subjected to rising damp for several centuries [35,36], in marine locations or in presence of salt contaminated underground water. There is no significant difference between the lower and the upper layers of the matrix (M-C-INT and M-C-EXT, respectively), which means that no accumulation of salts occurred in the mortar pores during the cycles and external efflorescence simply formed on the surface, which confirms the visual observations. Salts are present in the bricks in lower amounts than the matrix, but this seems mostly related to the higher salt amount present in the matrix with respect to the bricks before the cycles. Interestingly, the FRCM composite does not hinder the capillary flow of the saline solution, which in turn results in no accumulation of salts beneath the composite itself as observed by the authors in [24]. Salt accumulation beneath the composite could compromise adhesion. It is reasonable to state that the lower average load-carrying capacity of the SALT-DRY specimens, with respect to REF-DRY specimens has to be ascribed only to the presence of corrosion of the fibers, as other detrimental phenomena to the bond behavior associated with salt attack were not detected.

In the POST-DRY specimens, the amount of anions in the composite is high (1.3% for chloride and 1.6% for sulfate, on average), which highlights that the application of the composite to the already salt-contaminated blocks causes firstly a dissolution of the salts in the masonry (during the application and curing of the composite) and then their absorption (during drying). Hence, the application of FRCM composite on salt laden masonry may cause an immediate absorption of salts, even in the absence of further crystallization cycles, which leads to an anions concentration close to the one achieved after weathering cycles. This observation is in agreement with the single-lap test results, i.e. the load-carrying capacity of the SALT-DRY and POST-DRY specimens is similar.

#### **4.4.2. Pore size and pore distribution**

Results obtained by MIP analysis of fragments collected from the M-C-EXT layers are reported in Table 3, in terms of total open porosity and average pore radius.  $R_{av}$  in Table 3 is the radius corresponding to 50% of the intruded mercury volume.

The WATER-DRY sample is basically identical to the REF-DRY one, in terms of porosity and  $R_{av}$ , hence cycles in water have produced no additional effect on the matrix curing. This seems due to the fact that the curing of the FRCM composite was carried out in moist conditions and the hardening reactions of the hydraulic lime matrix were already boosted during the curing process.

Specimens subjected to cycles in saline solution (SALT-DRY) exhibit a total porosity of the matrix (21.5%) smaller than REF-DRY specimens (26.5%), as expected due to the fact that salts partially occlude the pores. However, the SALT-DRY sample also exhibits an average pore radius equal to 0.85  $\mu\text{m}$ , hence slightly larger than the REF-DRY sample ( $R_{av} = 0.49 \mu\text{m}$ ), which can be ascribed to the formation of some micro-cracks related to the salt crystallization cycles or, most likely, related to the corrosion of the steel embedded in the matrix. After desalination, SALT-DRY exhibits a porosity similar to REF-DRY specimens, as the salt crystals were removed, but the pore mean radius remains basically unaltered, which confirms the absence of micro-cracks.

Interestingly, the POST-DRY sample is characterized by the lowest porosity (17.4%) and the smallest mean pore radius (0.05  $\mu\text{m}$ ) among all series. In this case, the salts that migrated from masonry into the composite matrix precipitated inside the pores, causing a significant reduction of the porosity. The decrease of the pores size is due to the fact that thinner pores form among the precipitated salts crystals.

Table 3. Total open porosity and average pore radius ( $R_{av}$ ) of matrix samples extracted from REF-DRY, WATER-DRY, SALT-DRY and POST-DRY specimens.

Samples	Sampling locations (as in Fig. 4)	Total open porosity (%)	$R_{av}$ ( $\mu\text{m}$ )
REF-DRY	M-C-EXT	26.5	0.49
WATER-DRY	M-C-EXT	27.1	0.49
SALT-DRY	M-C-EXT	21.5	0.85
SALT-DRY (desalinated)	M-C-EXT	25.9	0.84
POST-DRY	M-C-EXT	17.4	0.05

## 5. Conclusions

In the present experimental campaign, steel FRCM-masonry joints were manufactured and subjected to a purposely designed accelerated weathering protocol, consisting of six wetting-drying cycles in an aqueous solution of sodium sulfate and sodium chloride. For comparison purposes, a set of FRCM-masonry joints was subjected to the same six wetting-drying cycles in deionized water and another one was not subjected to any cycles (but left at room conditions for the same period of time). First all specimens were tested to determine the bond capacity by using a single-lap shear test set-up, and then subjected to materials characterization. Moreover, with the aim of investigating the mechanical behavior of the FRCM composite in conditions as close as possible to the ones of real historical buildings, two further sets of specimens were investigated: a set of masonry blocks was firstly subjected to cycles in saline solution, then reinforced with the composite, and finally direct shear tests were performed; another set was subjected to cycles in water and then tested in water saturated conditions.

The results obtained allow to make the following remarks:

- The FRCM-masonry joints exhibited in almost all cases an interlaminar failure mode, which is quite typical for FRCM composites and consists of fracturing of the matrix layers as the fibers slip with respect to the matrix. Control specimens (REF-DRY) provided a load carrying capacity around 7 kN, while conditioned specimens (WATER-DRY, WATER-WET, SALT-DRY and POST-DRY) showed a load-carrying capacity, on average, of about 5.5 kN;
- Six wetting/drying cycles in deionized water (WATER-DRY) did not cause any increase in the bond capacity of the composite. This result was ascribed to the fact that the composite strips were cured for 28 days in wet conditions and this caused a fairly complete curing of the hydraulic lime, hence no further mechanical benefit was achieved by cycles in water;
- When tested in saturated conditions (WATER-WET), specimens exhibited a decrease of the bond capacity with respect to the REF-DRY ones (-30%). This decrease is higher, as expected, than the decrease of the bond capacity of the FRCM-masonry joints tested in dry conditions (WATER-DRY) due to the overpressures caused by the presence of water inside the pores;



- Six wetting/drying cycles in saline solution produced a remarkable amount of efflorescence on the surface of the specimens, especially over the composite strip and in the bricks near the strip itself. The amount of salts accumulated in the composite matrix is similar to that found in ancient masonry that has been affected by rising damp from the ground and/or marine aerosol spray for centuries;
- Due to the high porosity of the matrix (26.5%), salts did not accumulate beneath the composite, but migrated through the composite. Thus, no particular risk of detachment of the FRCM strip was envisaged. This aspect represents a key advantage of the FRCM composites with respect to FRPs, where the composite, due to the impermeability of the organic matrix, provides a barrier to the flow of the rising damp from the masonry substrate that may lead to possible bond degradation phenomena;
- The cycles in the saline solution (SALT-DRY) caused a decrease of the bond capacity with respect to REF-DRY specimens (-26%), but this decrease has to be ascribed only to the steel corrosion in presence of chloride rather than to the disruptive effect of salt crystallization cycles on the matrix. In fact, some corrosion was observed on the steel cords, while no increase of the total porosity was found in the matrix of the composite. Six salt crystallization cycles successfully produced a very high accumulation of salts in the pores, but no severe decay of the mechanical properties. The effect of increasing the numbers of cycles is currently under investigation;
- When applied to masonry blocks that had already undergone cycles in saline solution (POST-DRY), the FRCM composite exhibited a behavior very similar to the one that was found for the SALT-DRY specimens, where the composite was applied to the masonry blocks before the weathering protocol. In fact, during the application and curing, the matrix absorbed a large amount of salts from the substrate. The bond capacity decreases (-20% compared with REF-DRY specimens) and the presence of corrosion spots was similar to SALT-DRY specimens. This highlights that the concentration of chloride may have an impact on the bond capacity independently of the number

of crystallization cycles. This also highlights that applying the FRCM composite on salt-laden masonry may require some preliminary cleaning of the substrate.

The artificial weathering procedure described in Section 3.2 is aimed not only at contributing to the development of a standardized test to assess the long-term performance of FRCM-composites, but also to investigate the mechanisms of salts migration, accumulation, and crystallization across composite-masonry joints, and their influence on the load-carrying capacity. This aspect is very important to assess the behavior of the FRCM composites in real historical buildings and further tests are currently in progress with different types of FRCMs, in order to better shed light on this unexplored aspect. In fact, it is expected that the permeability of the composite matrix may alter significantly the salt migration and crystallization paths, thus leading to different damaging scenarios, which depend on the properties of the composite.

In conclusion, the results of the present experimental campaign are intended to increase the knowledge on the behavior of steel FRCM-masonry interfacial debonding in presence of moisture and salts. However, it is important to recognize that FRCM-masonry joints are characterized by a complex behavior that produces a high variability in the test outcomes, thus it is recommended that further research is conducted to confirm the results herein presented and to expand the database on the topic.

### **Acknowledgements**

The experimental work discussed in this paper was conducted at the University of Bologna. Technicians of the laboratory LISG (Laboratory of Structural and Geotechnical Engineering), CIRI (Interdepartmental Centre for Industrial Research in Building and Construction), LASTM (Laboratory of Materials Science and Technology) are gratefully acknowledged for their help during the preparation of the specimens and the execution of the tests. The authors would like to express their appreciation to Kerakoll S.p.A. (Sassuolo, Italy) for providing the composite materials. Mr. Leonardo Corona is gratefully acknowledged for his support during the experimental campaign. Financial support by the Italian Ministry of Education, Universities and Research MIUR is gratefully acknowledged (PRIN2015: "Advanced mechanical modeling of new materials and structures for the solution of 2020 Horizon challenges", prot. 2015JW9NJT 018).

## References

- [1] Castellazzi G, Gentilini C, Nobile L. Seismic vulnerability assessment of a historical church: Limit analysis and nonlinear finite element analysis (2013) *Advances in Civil Engineering*, art. no. 517454.
- [2] Cannizzaro F, Pantò B, Lepidi M, Caddemi S, Calò I. Multi-directional seismic assessment of historical masonry buildings by means of macro-element modelling: Application to a building damaged during the L'Aquila earthquake (Italy) (2017) *Buildings*, 7 (4), art. no. 106 .
- [3] Fiorentino G, Forte A, Pagano E, Sabetta F, Baggio C, Lavorato D, Nuti C, Santini S. Damage patterns in the town of Amatrice after August 24th 2016 Central Italy earthquakes (2018) *Bull Earthquake Eng* 16:1399-1423.
- [4] D'Altri AM, Castellazzi G, de Miranda S, Tralli A. Seismic-induced damage in historical masonry vaults: A case-study in the 2012 Emilia earthquake-stricken area (2017) *J Build Eng* 13:224-243.
- [5] Valente M, Barbieri G, Biolzi L. Damage assessment of three medieval churches after the 2012 Emilia earthquake (2017) *Bull Earthquake Eng* 15:2939-2980.
- [6] Valluzzi MR, Modena C, de Felice G. Current practice and open issues in strengthening historical buildings with composites (2014) *Mater Struct* 47:1971-1985.
- [7] Sassoni E, Sarti V, Bellini A, Mazzotti C, Franzoni E. The role of mortar joints in FRP debonding from masonry (2018) *Compos Part B-Eng* 135:166-174.
- [8] Freddi F, Sacco E. Debonding Process of masonry element strengthened with FRP (2015) *Procedia Engineering* 109:27-34.
- [9] Faella C, Camorani G, Martinelli E, Paciello SO, Perri F. Bond behaviour of FRP strips glued on masonry: Experimental investigation and empirical formulation (2012) *Constr Build Mater* 31:353-363.
- [10] Maljaee H, Ghiassi B, Lourenço PB, Oliveira DV. FRP–brick masonry bond degradation under hygrothermal conditions (2016) *Compos Struct* 147:143-154.
- [11] Ghiassi B, Lourenço PB, Oliveira DV. Effect of environmental aging on the numerical response of FRP-strengthened masonry walls (2016) *J Struct Eng* 142, art. no. 04015087.

- [12] Sciolti MS, Aiello MA, Frigione M. Influence of water on bond behavior between CFRP sheet and natural calcareous stones (2012) *Compos Part B-Eng* 43:3239-3250.
- [13] Babaeidarabad S, Caso FD, Nanni A. Out-of-plane behavior of URM walls strengthened with fabric-reinforced cementitious matrix composite (2014) *J Compos Constr* 18, art. no. 04013057
- [14] Papanicolaou CG, Triantafillou TC, Papathanasiou M, Karlos K. Textile reinforced mortar (TRM) versus FRP as strengthening material of URM walls: Out-of-plane cyclic loading (2008) *Mater Struct* 41:43-157.
- [15] Mordanova A, De Santis S, De Felice G. State-of-the-art review of out-of-plane strengthening of masonry walls with mortar-based composites (2016) *Structural Analysis of Historical Constructions: Anamnesis, diagnosis, therapy, controls - Proceedings of the 10th International Conference on Structural Analysis of Historical Constructions, SAHC 2016*, 337-343.
- [16] Franzoni E. Rising damp removal from historical masonries: A still open challenge (2014) *Constr Build Mater* 54:123-136.
- [17] Sandrolini F, Franzoni E. Repair systems for the restoration of ancient buildings – dampness rise problem (2007) *Rest Build Monument* 13:161–171.
- [18] Garavaglia E, Tedeschi C, Perego S, Valluzzi MR. Probabilistic modelling of the damage induced by salt crystallization in fiber reinforced clay brick masonry (2016) *Brick and Block Masonry: Trends, Innovations and Challenges - Proceedings of the 16th International Brick and Block Masonry Conference, IBMAC 2016*, 487-494.
- [19] Cardani G, Valluzzi MR, Panizza M, Girardello P, Binda L. Influence of salt crystallization on composites-to-masonry bond evaluated on site by pull-off tests (2015) *Key Eng Mater* 624:338-345.
- [20] Arboleda D, Babaeidarabad S, DiLaurenzio Hays C, Nanni A. Durability of Fabric Reinforced Cementitious Matrix (FRCM) composites (2014) *Proceedings of the 7th International Conference on FRP Composites in Civil Engineering, CICE*.

- [21] Donnini J, De Caso y Basalo F, Corinaldesi V, Lancioni G, Nanni A. Fabric-reinforced cementitious matrix behavior at high-temperature: Experimental and numerical results (2017) *Compos Part B-Eng* 108:108-121.
- [22] Doehne E. Salt weathering: a selective review (2002) *Geol Soc Spec Publ* 205: 51-64.
- [23] Charola AE. Salts in the deterioration of porous materials: an overview (2000) *J Am inst Cosnserv* 39:327–343.
- [24] Franzoni E, Gentilini C, Santandrea M, Zanotto S, Carloni C. Durability of steel FRCM-masonry joints: effect of water and salt crystallization (2017) *Mater Struct* 50, art. no. 201.
- [25] EN 772–1 Methods of test for masonry units - Part 1: Determination of compressive strength, 2015.
- [26] EN 998-2 Specification for mortar for masonry - Part 2: Masonry mortar, 2016.
- [27] Kerakoll 2017. Technical data sheet Biocalce Muratura. <http://products.kerakoll.com/gestione/immagini/prodotti/00339bio%20muratura%202013.pdf>
- [28] EN 1015–11 Methods of test for mortar for masonry - Part 11: Determination of flexural and compressive strength of hardened mortar, 1999.
- [29] Kerakoll 2016. Technical data sheet GeoSteel G600. <http://products.kerakoll.com/gestione/immagini/prodotti/00075GeoSteel%20G600%202016.pdf>
- [30] Gentilini C, Franzoni E, Bandini S, Nobile L. Effect of salt crystallisation on the shear behaviour of masonry walls: An experimental study (2012) *Constr Build Mater* 37:181-189.
- [31] Franzoni E, Gentilini C, Graziani G, Bandini S. Towards the assessment of the shear behaviour of masonry in on-site conditions: A study on dry and salt/water conditioned brick masonry triplets (2014) *Constr Build Mater* 65:405-416.
- [32] EN 12370 Natural stone test methods - Determination of resistance to salt crystallization, 1999.
- [33] RILEM TC 127-MS MS-A.1 - Determination of the resistance of wallettes against sulphates and chlorides (1998) *Mater Struct* 31:2–9.
- [34] RILEM TC 127-MS MS-A.2 - Unidirectional salt crystallization test for masonry units (1998) *Mater Struct* 31:10–11.

- [35] Sandrolini F, Franzoni E, Cuppini G, Caggiati L. Materials decay and environmental attack in the Pio Palace at Carpi: a holistic approach for historical architectural surfaces conservation (2007) *Build Environ* 42:1966–1974.
- [36] Sandrolini F, Franzoni E. Characterization procedure for ancient mortars' restoration: the plasters of the Cavallerizza courtyard in the Ducal Palace in Mantua (Italy) (2010) *Mater Characterization* 61:97-104.
- [37] Franzoni E, Bandini S, Graziani G. Rising moisture, salts and electrokinetic effects in ancient masonries: From laboratory testing to on-site monitoring (2014) *J Cult Herit* 15:112-120.
- [38] Franzoni E, Gentilini C, Graziani G, Bandini S. Compressive behaviour of brick masonry triplets in wet and dry conditions (2015) *Constr Build Mater* 82:45-52.
- [39] Verstryngge E, Adriaens R, Elsen J, Van Balen K. Multi-scale analysis on the influence of moisture on the mechanical behavior of ferruginous sandstone (2014) *Constr Build Mater* 54:78–90
- [40] Santandrea M, Daissè G, Mazzotti C, Carloni C. An investigation of the debonding mechanism between FRCM composites and a masonry substrate (2017) *Key Eng Mater* 747:382-389.
- [41] D'Antino T, Pellegrino C, Carloni C, Sneed LH, Giacomini G. Experimental analysis of the bond behavior of glass, carbon, and steel FRCM composites (2014) *Key Eng Mater* 624:371-378.
- [42] Carloni C, D'Antino T, Sneed LH, Pellegrino C. Role of the matrix layers in the stress-transfer mechanism of FRCM composites bonded to a concrete substrate (2015) *J Eng Mech* 141:04014165-1-04014165-10.
- [43] D'Antino T, Sneed LH, Carloni C, Pellegrino C. Effect of the inherent eccentricity in single-lap direct-shear tests of PBO FRCM-concrete joints (2016) *Compos Struct* 142:117-129.
- [44] D'Antino T, Carloni C, Sneed LH, Pellegrino C. Matrix-fiber bond behavior in PBO FRCM composites: a fracture mechanics approach (2014) *Eng Fract Mech* 117:94-111.
- [45] Pernicova R, Dobias D, Pokorny P. Problems connected with use of hot-dip galvanized reinforcement in concrete elements (2017) *Procedia Engineering* 172:859 – 866.
- [46] Murakami K, Kanematsu H, Nakata K. Corrosion characteristics in concrete environment of hot dip galvanized steel and Zn alloy hot dip coated steel (2009) *T I Met Finish* 87:23-27.

- [47] Bellezze T, Fratesi R, Tittarelli F. Corrosion behaviour of galvanized steel rebars in the presence of coating discontinuities (2006) *Corrosion of Reinforcement in Concrete: Monitoring, Prevention and Rehabilitation Techniques*, 27-37.
- [48] Roventi G, Bellezze T, Giuliani G, Conti C. Corrosion resistance of galvanized steel reinforcements in carbonated concrete: effect of wet–dry cycles in tap water and in chloride solution on the passivating layer (2014) *Cement Concrete Res* 65: 76–84.
- [49] Fayala I, Dhouibi L, Nóvoa XR, Ben Ouezdou M. Effect of inhibitors on the corrosion of galvanized steel and on mortar properties (2013) *Cement Concrete Comp* 35:181–189.
- [50] Yadav AP, Nishikata A, Tsuru T. Degradation mechanism of galvanized steel in wet–dry cyclic environment containing chloride ions (2004) *Corros Sci* 46:361–376
- [51] Del Angel E, Vera R, Corvo F. Atmospheric corrosion of galvanized steel in different environments in Chile and Mexico (2015) *Int J Electrochem Sci*:10:7985 – 8004.